

Catalysis Science & Technology

Design of Low Temperature La2O3 Oxidative Coupling of Methane Catalysts using Feature Engineering and Automated Sampling

Journal:	Catalysis Science & Technology		
Manuscript ID	CY-ART-09-2024-001142.R1		
Article Type:	Paper		
Date Submitted by the Author:	25-Oct-2024		
Complete List of Authors:	Escobar, Fernando; Hokkaido University, Department of Chemistry Takahashi, Lauren; Hokkaido University, Nishimura, Shun; Japan Advanced Institute of Science and Technology, Graduate School of Advanced Science and Technology Takahashi, Keisuke; Hokkaido University, Department of Chemistry Shaaban, Ali; Hokkaido University, Department of Chemistry		

SCHOLARONE™ Manuscripts

Journal Name



ARTICLE TYPE

Cite this: DOI: 10.1039/xxxxxxxxxx

Design of Low Temperature La₂O₃ Oxidative Coupling of Methane Catalysts using Feature Engineering and Automated Sampling

Fernando Garcia-Escobar a* , Lauren Takahashi a , Ali Shaaban a , Shun Nishimura c , Keisuke Takahashi ab*

Received Date
Accepted Date

DOI: 10.1039/xxxxxxxxxxx

www.rsc.org/journalname

The design of efficient catalysts remains an challenge for complex systems such as the Oxidative Coupling of Methane (OCM), where reaction mechanisms are still debated. Catalysts informatics workflows have proved useful in identifying high-performing material candidates and optimizing reaction conditions from underlying trends in experimental data. Herein, a data set composed La₂O₃supported catalysts for the OCM reaction is used to construct a Support-Vector Regression (SVR) model and extract four element combinations to support on La₂O₃ and test for low temperature catalytic activity, with the best result observed for (Y, Cs)/La₂O₃. This methodology presents an effective approach from building a regression model using engineered features with an automated sampling technique to the extraction and experimental validation of promising catalyst candidates, which can also be extended toward other catalytic reactions.

1 Introduction

Methane is an abundant resource that has been used for both the production of higher-value chemicals and in fuel applications. Although the direct synthesis of C_2 hydrocarbons from methane was proposed more than forty years ago 1 , the high stability of the C-H bond remains an obstacle to this day, since the conversion of a methane molecule to a methyl radical is the starting point of the

reaction². The need for highly selective catalysts is widely understood, as the formation of deep oxidation products is more thermodynamically-favored at higher temperatures³. Catalyst-assisted mechanism studies have also been carried out, as the reaction pathways depend directly on the catalyst surface's structure, chemistry and the process conditions^{4–9}. However, to this day, a definitive mechanism has not been elucidated, which leaves structure-activity relationships unclear.

Among the various metal oxides that have been studied as suitable OCM catalysts, lanthanum oxide (La₂O₃) has shown good activity and high selectivity for C2 products at relatively low temperatures ¹⁰ that can be improved with the addition of promoter elements 11-18. These properties make it a good candidate as a support material for low temperature catalysts. In recent years, datadriven approaches have been adopted to propose and test new catalyst systems as an attempt to increase overall C₂ yield. Starting from literature data ^{19–24}, first-principle calculations ^{25–27} to high-throughput experimentation approaches ^{28–34}, data-driven approaches have proven successful in proposing and uncovering new active OCM catalysts and experimental conditions 35 that improve C₂ yield. Nevertheless, the complete optimization of this reaction remains unsolved, as it involves the reactions occurring gas phase ³⁶, the surface reactions on the catalyst surface ^{8,37}, the nature of the catalyst surface ^{2,38,39} and the inclusion of additional elements through procedures such as impregnation that change the nature of the catalyst's surface $^{13-15}$.

This work presents a Machine Learning-assisted approach to design descriptors (features) that represent catalyst composition to predict C_2 yield as a function of reaction temperature and extract impregnated element combinations to enhance the C2 yield for the low temperature La_2O_3 OCM activity. For simplicity, the analyzed data set fixes the metallic oxide support, supported element amount and reaction gas flow conditions, leaving the identity of the supported elements and reaction temperature as the only variables to optimize towards low temperature-high C_2 yield.

^a Department of Chemistry, Hokkaido University, North 10, West 8, Sapporo 060-0810, Japan

b List Sustainable Digital Transformation Catalyst Collaboration Research Platform, Institute for Chemical Reaction Design and Discovery, Hokkaido University, Sapporo 001-0021. Japan

^c Graduate School of Advanced Science and Technology, Japan Advanced Institute of Science and Technology, 1–1 Asahidai, Nomi, Ishikawa 923–1292, Japan

^{*} email:escobarfernando.garcia.u8@elms.hokudai.ac.jp

^{*} email:keisuke.takahashi@sci.hokudai.ac.jp

 $[\]dagger$ Electronic Supplementary Information (ESI) available: [details of any supplementary information available should be included here]. See DOI: 10.1039/b000000x/

2 Methodology

Data handling, processing, analysis and visualization are done with Python (v. 3.10.12), and the Scikit-learn library (v. 0.23.2) is implemented for ML procedures ⁴⁰.

2.1 Data set

The data set employed for this study (from here on referred to as the training data) to develop first-order features has been reported by Nishimura et al⁴¹, with this work focusing only on the catalysts tested under the same gas flow conditions with a feed composed of $CH_4:O_2:Ar$ at 66.7%, 22.6% and 9.7% vol., respectively. The data set is composed of 429 data points pertaining to 34 La_2O_3 -supported Oxidative Coupling of Methane (OCM) reaction activity and their observed C_2 yield (%) across 500-850 °C. The catalysts correspond to equimolar binary and ternary combinations of impregnated metallic elements and expressed as $M_1 \cdots M_n/La_2O_3$, where M_1 to M_n correspond to elements selected from Ba, Ca, Ce, Eu, K, La, Li, Mg, Mo, Na, Sm, Sr, Ti and W.

2.2 Data Analysis and Method

OCM Catalyst C_2 yield (%) is predicted with a Support-Vector Regression (SVR) model implemented with the radial basis function (RBF) kernel. To evaluate the performance of the regression models, a train-test split (80:20) is used to cross validate the predictions, with the evaluation metric being the average r^2 Score of the test data of data splits over random states 0-9. Hyperparameter values (C = 10, $\gamma = 0.01$) are optimized to avoid overfitting.

2.3 Reagents

Lanthanum (III) oxide (La_2O_3 , > 99%) purchased from Tokyo Chemical Industry, Co., Ltd. is used as support for the prepared catalysts. Potassium (KNO_3 , \geq 99%) and yttrium ($Y(NO_3)_3 \cdot 6H_2O$, 99%) nitrates from Junsei Chemical Co. Ltd., lithium (LiNO₃, 99%), cesium ($CsNO_3$, 99%) and cerium (III) ($Ce(NO_3)_3 \cdot 6H_2O$, special grade) nitrates from Wako Pure Chemical Corporation and europium (III) nitrate ($Eu(NO_3)_3 \cdot 5H_2O$, 99.9%) from Sigma Aldrich are used as impregnation precursors for the tested catalysts. All reagents are used without further purification.

2.4 Experimental Methodology

La₂O₃-supported catalysts are prepared based on a modified impregnation methodology previously reported by Nishimura et al 41 . The tested catalysts are prepared by impregnating La₂O₃ with water-soluble metallic nitrate precursors in the combinations presented on Table 1. In each instance, 2 g of La₂O₃ are dispersed in 100 mL of water and kept under continuous stirring. In parallel, 0.2 mmol of each metallic nitrate precursor are each separately dissolved in 50 mL of water and the solutions subsequently added to the La₂O₃ dispersion in increasing order of the precursors' metallic element atomic number, which is the same left-to-right order the elements are listed on Table 1. For example, in the case of Cat1, the order of addition is first Y(NO₃)₃, then CsNO₃. The resulting mixture is then allowed to age for 14 h without stirring at room temperature. The stirring is restarted

Table 1 Catalyst supported metal $(M_1, M_2, M_3)/La_2O_3$ combinations tested for OCM performance.

Label	\mathbf{M}_1	\mathbf{M}_2	\mathbf{M}_3
Cat1	Y	Cs	None
Cat2	Cs	Ce	None
Cat3	Li	K	Eu
Cat4	K	Y	Cs

after this period and water is evaporated at 70 °C. The remaining powder is then collected and dried at 120 °C for 2 h. Lastly, the material is then ground in a mortar, calcined at 700 °C for 3 h and ground again before testing.

Catalyst performance is tested in a steel fixed-bet tubular reactor (L = 262 mm, ID = 7.05 mm, SUS316L) from MECAFARM CO., LTD.. The catalyst powder (100 mg) is placed between two layers of quartz wool (5 mg each), with the catalyst layer located 97 mm from the top, and 165 mm from the bottom of the tube. The reactor temperature is monitored using a K-type thermocouple, with the tip placed near the outer reactor wall of the catalyst bed location. Prior to each measurement run, the system is purged at 300 °C for 30 min. under N2 gas at a flow of 30 SCCM to flush out all environmental gases that may interfere with the measurement. The system is then cooled to room temperature under the same flow conditions to start the catalyst performance measurements. The performance is studied at 450-700 °C at 50 °C intervals under a CH₄/O₂/N₂ flow at 18/9/3 SCCM, respectively. The reactor mixture is analyzed after an exposition time of 8 min for each temperature using a Shimadzu GC-2014 chromatograph equipped with a SHINCARBON ST 50/80 mesh column (3 mm x 2 m, He carrier). Gas conversion and product yield are estimated using N₂ as an internal standard. Reagent R conversions for O₂ and CH₄ are calculated in accordance to Equation (1). Product P yield for CO, CO₂, C₂H₄ and C₂H₆ is calculated in accordance to Equation (2), where n = 1 for CO and CO₂, and n = 2 for C₂H₄ and C₂H₆. Lastly, C₂ yield and selectivity are calculated according to Equations (3) and (4), respectively.

$$R_{Conv} = \frac{(R_{In}/N_{2In}) - (R_{Out}/N_{2Out})}{(R_{In}/N_{2In})} *100$$
 (1)

$$P_{Yield} = \frac{n(P_{Out}/N_{2Out})}{(CH_{4In}/N_{2In})} * 100$$
 (2)

$$C_{2vield} = C_2 H_{4Yield} + C_2 H_{6Yield} \tag{3}$$

$$C_{2selectivity} = \frac{C_{2yield}}{CH_{4Conv}} * 100 \tag{4}$$

3 Results and Discussion

The data set is composed of 429 data points pertaining to 34 La_2O_3 -supported OCM catalysts tested across 500-850 °C. The elements supported on La_2O_3 are presented on Figure 1 and belong to groups 1, 2, 4 and 5 of the Periodic Table, along with four Lanthanide group elements. Since the feed gas and the impregnated elements' composition are constant, the objective of the regres-

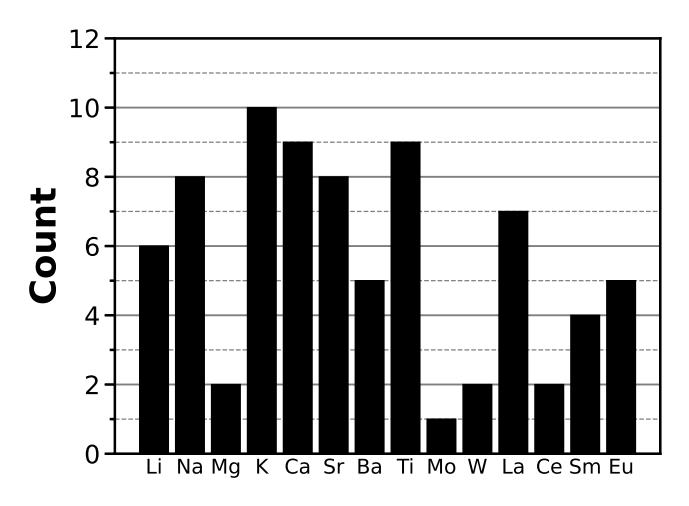


Fig. 1 Frequency count of the individual La_2O_3 -supported metallic elements in the catalysts within the training data.

sion model is to predict C_2 yield as a function of supported metals' combination (M_1, M_2, M_3) and reaction temperature.

An SVR model is employed to predict C2 yield as a function of catalyst composition and reaction temperature. Catalyst composition-related base features are calculated in accordance to Equation 5, where the features D are the aritmethic mean of 58 reference values D_i of each of the supported metallic elements ipresent in the La2O3 catalyst. Said reference values for the included elements are compiled in the XenonPy library 42 and a brief description for them is included in the Supporting Information as Table S1. Arithmetic mean values are considered in this case due to all catalysts containing supported metals present in equimolar amounts respective to each other. For example, a calculated atomic radius feature of a catalyst impregnated with Sr and Ce would be represented as the average of the atomic radii of Sr and Ce. Lastly, multiple analogues of the compositional base features are engineered by calculating the square, cubic, square root, exponential, and natural logarithm values along with their reciprocals to incorporate different feature scales that may adjust better to predict C₂ yield. After this step, the total number of feature increases from 59 to 639, as reaction temperature analogues are not engineered.

$$D = \frac{\sum_{i=1}^{n} D_i}{n} \tag{5}$$

Feature selection is carried out through the MonteCat algorithm algorithm previously reported 43 , where a regression model's cross validation $\rm r^2$ score is sought to be maximized through sequential randomized feature additions and removals across many iterations. In case a randomized feature inclusion or removal lowers the model's cross validation score, the implementation of this action is decided based on a computed probability P value as depicted in Equation 6 from a Boltzmann distribution that depends on the score's evolution $\Delta \rm r^2$ and a fixed MC Temperature T parameter value that regulates the leniency of implementing score-reducing actions. The algorithm is implemented for 10^4 iterations using $\{5,10,20,50,100,200,500,1000,2000\}$ values for the MC Temperature parameter. As a final note, it is pointed out

Table 2 Extracted supported metal combinations with the highest predicted C_2 yield at 650 °C.

M1	M2	М3	Pred. C ₂ y (%)
Y	Cs	-	15.90
K	Ba	-	15.90
Cs	Ce	-	15.77
Ba	Th	-	15.68
Ba	Pr	-	15.66
Li	K	Eu	16.03
K	Y	Cs	15.89
K	Cs	Ce	15.86
Y	Cs	Ba	15.84
K	Cs	Tm	15.82

that this MonteCat Temperature parameter has no relation to the experimental reaction Temperature that takes part as one of the features in the regression model. A detailed workflow is included in the Supporting Information as Figures S1 and S2.

$$P(\Delta r^2) = e^{\frac{\Delta r^2}{k_B T}} \tag{6}$$

The results of the feature selection procedure are presented on Figure 2. Twenty five runs with different fixed random seed values are carried out for each depicted temperature value, and after the completion of each run, the highest observed score throughout the run is identified along with the feature subset at that point. A cross-validation score greater than 0.9 is consistently observed throughout all experiments (a), and a subset containing 15 features is extracted to be used in the prediction model (b), with the best test r² score of 0.9403 (c).

From this point, this subset is used to carry out a Sequential Feature Elimination (SFE) procedure to remove features that do not help increase the model's predictive accuracy. The results are presented on Figure 3, where it can be observed that having only 5 features allows the SVR model to reach a test r^2 score > 0.9. The features selected for the regression model are analogues of the atomic weight, covalent radius, number of valence electrons on the s shell, Van der Waals radius and the reaction temperature.

An inverse prediction at 650 °C contemplating all binary and ternary combinations from Li, Na, Mg, K, Ca, Sc, Ti, V, Cr, Mn, Fe, Co, Ni, Cu, Zn, Rb, Sr, Y, Zr, Nb, Mo, Ru, Rh, Pd, Ag, Cd, Cs, Ba, La, Ce, Pr, Nd, Sm, Eu, Gd, Tb, Dy, Ho, Er, Tm, Yb, Lu, Hf, Ta, W, Re, Os, Ir, Pt, Au and Hg, which belong to blocks s, d and f of the Periodic Table is carried out. This results in 22,101 supported metal combinations whose C_2 yield is predicted at 650 °C using the constructed SVR model. Table 2 presents the results for the five highest binary and ternary combinations from which the best two performing binary and ternary combinations are selected, prepared and tested experimentally. On an additional note, K/Ba is not tested due to that pair already being included in the training data.

The average results for three measurements for Cat1-4 are presented on Figure 4, where a Blank (the reaction carried out without catalyst inside) and La_2O_3 without supported metals are included as reference. The behavior observed without catalytic ma-

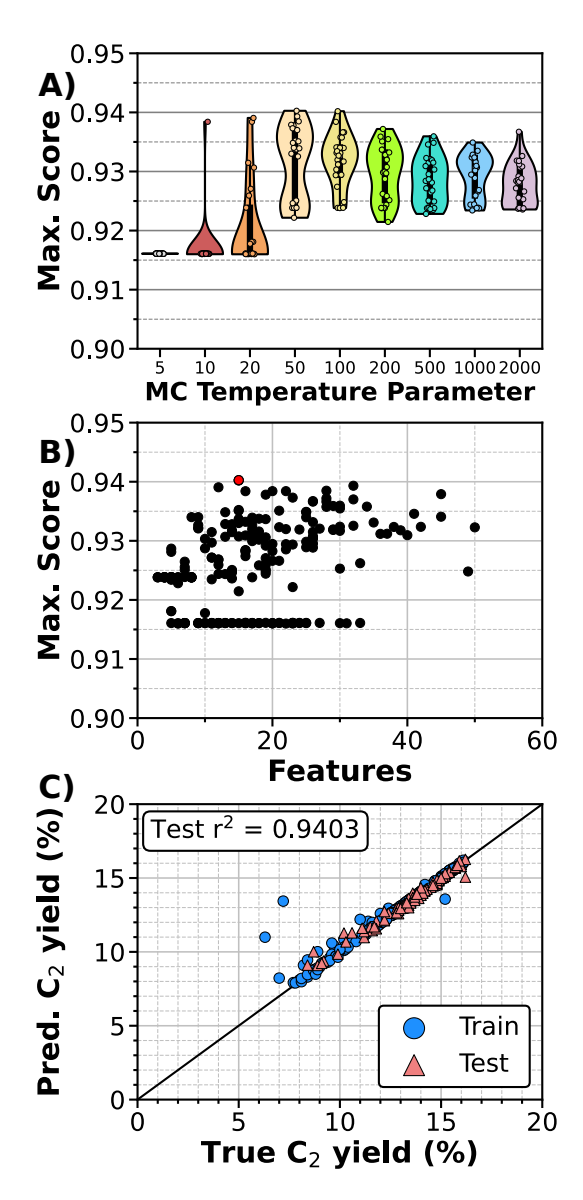


Fig. 2 MonteCat process-extracted feature subsets' performance with a SVR (C = 10, γ = 0.01) model across various Temperature parameter values (a), score-feature number behavior with the best-performing subset highlighted in red (b) and parity plot of the feature subset with the highest observed score (c).

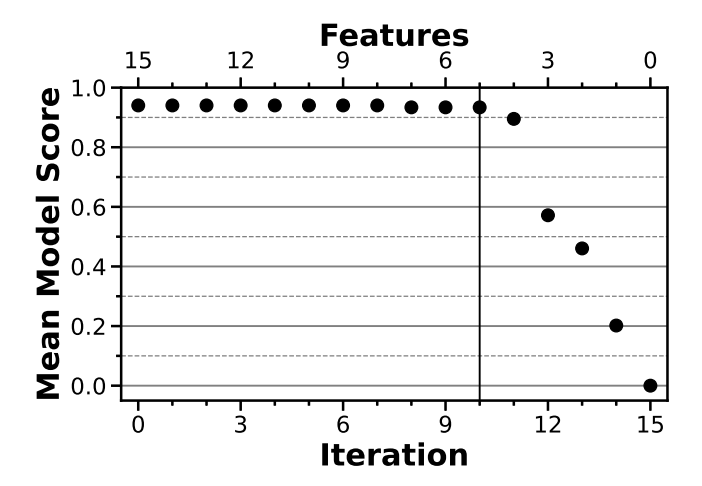


Fig. 3 Backward Feature Elimination procedure results applied upon the MonteCat-extracted feature subset derived from the highest observed cross validation $\rm r^2$ score. The vertical guide line represents the spot where the features stopped being removed, leaving the final model with 5 only features.

terial is a steady increase in O_2 and CH_4 conversion, which could be attributable to CH_4 oxidation taking place in gas phase and along the reactor walls 44,45 . While the CH_4 conversion increases steadily, there is an abrupt increase in O_2 conversion between 650-700 °C also observed in CH_4 and CO_2 conversions. Starting at 650 °C, C_2H_6 is detected, which indicates that oxidative coupling starts around this temperature range with low C_2 selectivity (<5%). When pure La_2O_3 is tested instead, O_2 and CH_4 conversions increase at lower temperatures due to La_2O_3 contributing to CH_4 oxidation 10,11,46 . In the same manner, CO_2 yield is greater than the one observed in the absence of catalyst and C_2H_4 and C_2H_6 are both produced starting at 600 °C, although the highest observed C_2 yield (at 650 °C) reached 1.5 % with a C_2 selectivity of 11%.

This behavior is enhanced with the presence of supported metals. Both Cat1 and Cat2 display similar O2 and CH4 conversion output, but Cat1 reaches a 100 % O2 conversion at 600 °C, while Cat2 does so at 650 °C. Both catalysts reach their maximum C2 vield at 650 °C at values around 6 % and 3.7 % with selectivities of 31.8 % and 20.5 % for Cat1 and Cat2, respectively. The ternary catalysts Cat3 and Cat4 display different behavior from their binary counterparts. Cat3 displayed generally lower or equal O2 conversion compared to the Blank across the entire temperature range, while Cat4 behaved in a similar manner to the Blank, with the only noteworthy difference is a larger O₂ conversion at 650 °C. For both ternary catalysts, the peak activity is observed at 700 °C, with Cat3 showing higher C2 yield and selectivity (4.9 % and 23.4 %, respectively) than Cat4 (2.6 % and 13.6 %, respectively). Interestingly, Cat3 is the only material that exhibited equal or lower reagent conversions compared to the results observed in the absence of catalyst. Measurements at temperatures higher than 700 °C are not included, as only CO_x products are detected possibly due to the SUS316 reactor becoming catalytically-active.

The catalytic activity of the tested materials can be better observed on Figure 5 by comparing C₂ selectivity versus CH₄ con-

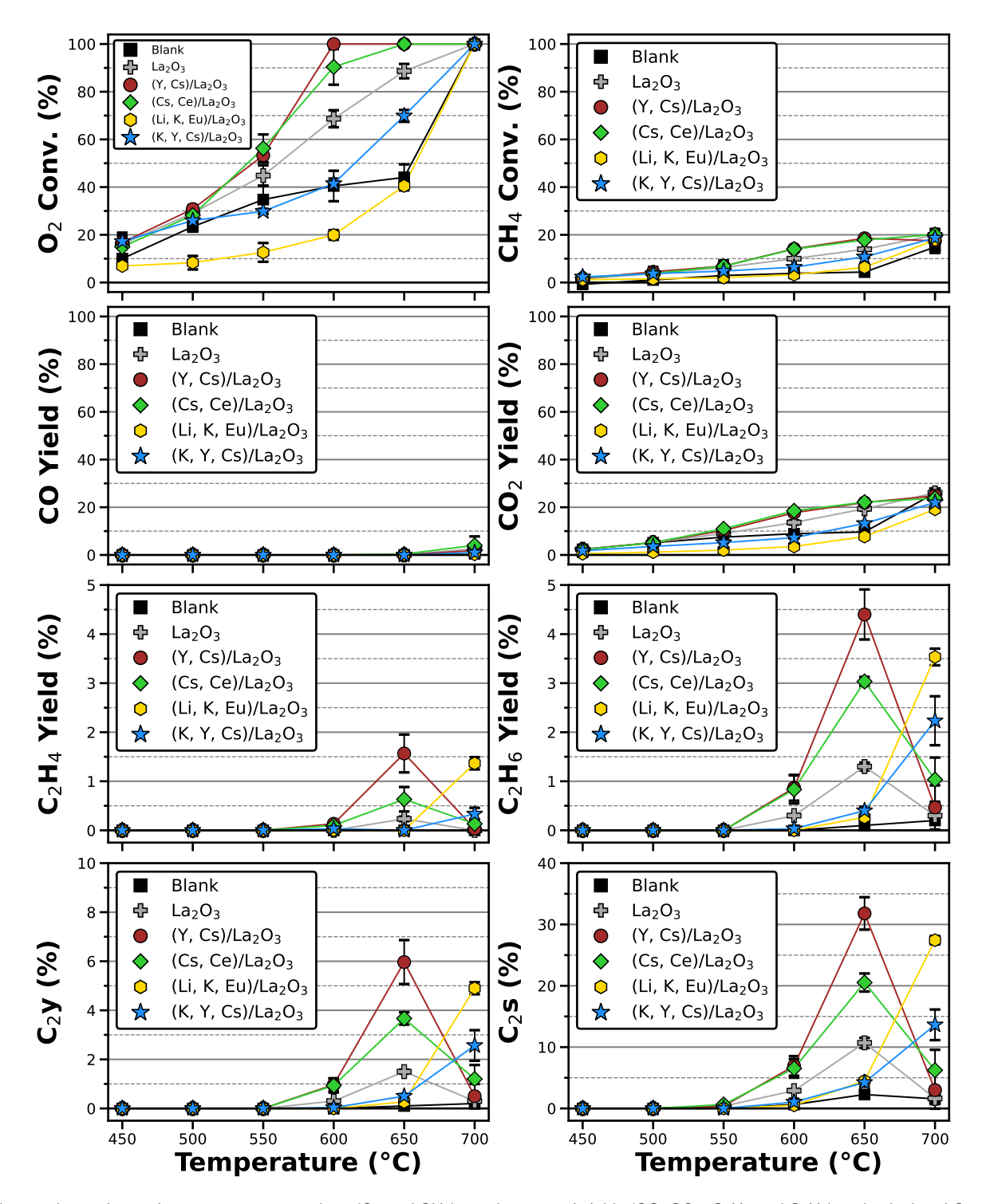
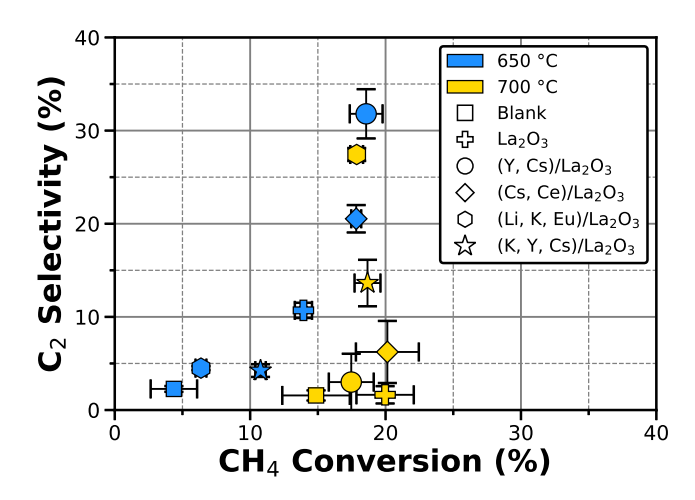


Fig. 4 Observed experimental reagent gas conversions (O_2 and CH_4), product gases' yields (CO, CO_2 , C_2H_4 and C_2H_6) and calculated C_2 yields and selectivities at the bottom for each tested catalyst respective to the reaction temperatures. The depicted values represent an average across three runs, with error bars depicting the standard deviation of the measurements.



version. At temperatures below 600 °C, no C_2 products are detected even though there is CH_4 conversion, resulting in a direct conversion into CO_2 . The binary catalysts indeed display both, a higher CH_4 conversion with higher C_2 selectivities at lower temperatures. Nevertheless, OCM activity decreases at 700 °C for La_2O_3 and Cat1-2, while Cat3-4 show higher activity at this temperature, with Cat3 achieving slightly lower C_2 selectivity than Cat1 at roughly the same CH_4 conversion.

4 Conclusion

This study presents a Machine Learning-assisted methodology to uncover low temperature OCM catalysts. Feature design and selection, catalyst prediction and experimental testing are all carried out, resulting in four impregnated metal combinations that boost La₂O₃ OCM activity in the 650-700 °C range. The best performance is observed on (Y, Cs)/La₂O₃ with a C₂ selectivity at 32% with 18% CH₄ conversion at 650 °C. This methodology presents an effective first approach at constructing regression models solely from catalyst composition and reaction conditions. New and efficient combinations of metals can then be characterized further to establish structure-property relationships that can then be used to elucidate reaction mechanisms.

5 Supporting Information

Further details on the base features and the feature engineering and selection steps are included as Supporting Information.

6 Acknowledgment

This work is funded by the Japan Science and Technology Agency (JST) CREST Grant Number (JPMJCR17P2), ERATO grant number (JPMJER1903), PRESTO grant number (JPMJPR24T5). JST Mirai Program Grant Number (JPMJMI22G4), JSPS KAKENHI Grant-in-Aid for Scientific Research (B) Grant Number (JP23H01762) and (24K01241).

The authors would also like to acknowledge the technical support from Mr. Masato Ishii and Mr. Shigehiro Umegai from MECA-FARM CO., LTD..

7 Data Availablility

The training data set used in this study and the feature lists for the highest-scoring subsets presented on Figure 2 are available.

8 Conflict of Interest Disclosure

The authors declare no competing financial interest.

Notes and references

- 1 Keller, G.; Bhasin, M. Synthesis of ethylene via oxidative coupling of methane: I. Determination of active catalysts. *J. Catal.* **1982**, *73*, 9–19.
- 2 Noon, D.; Seubsai, A.; Senkan, S. Oxidative Coupling of Methane by Nanofiber Catalysts. *ChemCatChem* **2013**, *5*, 146–149.
- 3 Farrell, B. L.; Igenegbai, V. O.; Linic, S. A Viewpoint on Direct Methane Conversion to Ethane and Ethylene Using Oxidative Coupling on Solid Catalysts. *ACS Catal.* **2016**, *6*, 4340–4346.
- 4 Takanabe, K.; Iglesia, E. Mechanistic Aspects and Reaction Pathways for Oxidative Coupling of Methane on Mn/Na2WO4/SiO2 Catalysts. *J. Phys. Chem. C* **2009**, *113*, 10131–10145.
- 5 Karakaya, C.; Zhu, H.; Zohour, B.; Senkan, S.; Kee, R. J. Detailed Reaction Mechanisms for the Oxidative Coupling of Methane over La2O3/CeO2 Nanofiber Fabric Catalysts. *Chem-CatChem* 2017, 9, 4538–4551.
- 6 Si, J.; Zhao, G.; Sun, W.; Liu, J.; Guan, C.; Yang, Y.; Shi, X.-R.; Lu, Y. Oxidative Coupling of Methane: Examining the Inactivity of the MnO-Na2WO4/SiO2 Catalyst at Low Temperature. *Angew. Chem., Int. Ed. Engl.* **2022**, *61*, e202117201.
- 7 Sourav, S.; Wang, Y.; Kiani, D.; Baltrusaitis, J.; Fushimi, R. R.; Wachs, I. E. New Mechanistic and Reaction Pathway Insights for Oxidative Coupling of Methane (OCM) over Supported Na2WO4/SiO2 Catalysts. *Angew. Chem., Int. Ed. Engl.* 2021, 60, 21502–21511.
- 8 Hu, L.; Pinto, D.; Urakawa, A. Catalytic Oxidative Coupling of Methane: Heterogeneous or Homogeneous Reaction? *ACS Sustainable Chem. Eng.* **2023**, *11*, 10835–10844.
- 9 Miyazato, I.; Nguyen, T. N.; Takahashi, L.; Taniike, T.; Takahashi, K. Representing Catalytic and Processing Space in Methane Oxidation Reaction via Multioutput Machine Learning. J. Phys. Chem. Lett. 2021, 12, 808–814.
- 10 Campbell, K. D.; Zhang, H.; Lunsford, J. H. Methane activation by the lanthanide oxides. *The Journal of Physical Chemistry* **1988**, *92*, 750–753.
- 11 DeBoy, J. M.; Hicks, R. F. The oxidative coupling of methane over alkali, alkaline earth, and rare earth oxides. *Industrial & Engineering Chemistry Research* **1988**, *27*, 1577–1582.
- 12 Choudhary, V. R.; Uphade, B. S.; Mulla, S. A. R. Oxidative Coupling of Methane over a Sr-Promoted La2O3 Catalyst Supported on a Low Surface Area Porous Catalyst Carrier. *Industrial & Engineering Chemistry Research* 1997, 36, 3594–3601.
- 13 Choudhary, V. R.; Mulla, S. A. R.; Rane, V. H. Surface basicity and acidity of alkaline earth-promoted La2O3 catalysts and their performance in oxidative coupling of methane. *JCTB*

- **1998**, 72, 125-130.
- 14 Choudhary, V.; Rane, V.; Chaudhari, S. Influence of various promoters on the basicity and catalytic activity of MgO catalysts in oxidative coupling of methane. *Catal. Letters* **1990**, *6*, 95–98.
- 15 Okabe, K.; Sayama, K.; Kusama, H.; Arakawa, H. Effects of Additives on SrO-La2O3 Catalysts for Oxidative Coupling of Methane. *JJPI* **1995**, *38*, 267–272.
- 16 Wang, Y.; Yang, X.; Yin, F.; Zhang, K.; Guo, H.; Wang, G.; Jiang, G.; Li, C.; Zhu, X. Elucidating the effect of barium halide promoters on La2O3/CaO catalyst for oxidative coupling of methane. *J. Energy Chem.* **2022**, *73*, 49–59.
- 17 Xiong, J.; Yu, H.; Wei, Y.; Xie, C.; Lai, K.; Zhao, Z.; Liu, J. Metal Ions (Li, Mg, Zn, Ce) Doped into La2O3 Nanorod for Boosting Catalytic Oxidative Coupling of Methane. *Catalysts* **2022**, *12*.
- 18 Ferreira, V. J.; Tavares, P.; Figueiredo, J. L.; Faria, J. L. Ce-Doped La2O3 based catalyst for the oxidative coupling of methane. *Catal. Commun.* **2013**, *42*, 50–53.
- 19 Zavyalova, U.; Holena, M.; Schlögl, R.; Baerns, M. Statistical Analysis of Past Catalytic Data on Oxidative Methane Coupling for New Insights into the Composition of High-Performance Catalysts. *ChemCatChem* 2011, 3, 1935–1947.
- 20 Kondratenko, E. V.; Schlüter, M.; Baerns, M.; Linke, D.; Holena, M. Developing catalytic materials for the oxidative coupling of methane through statistical analysis of literature data. *Catal. Sci. Technol.* 2015, 5, 1668–1677.
- 21 Suzuki, K.; Toyao, T.; Maeno, Z.; Takakusagi, S.; Shimizu, K.i.; Takigawa, I. Statistical Analysis and Discovery of Heterogeneous Catalysts Based on Machine Learning from Diverse Published Data. ChemCatChem 2019, 11, 4537–4547.
- 22 Zeng, D.; Song, Y.; Wang, M.; Lu, Y.; Chen, Z.; Xiao, R. A machine learning approach for predicting the performance of oxygen carriers in chemical looping oxidative coupling of methane. Sustainable Energy Fuels 2023, 7, 3464–3470.
- 23 Schmack, R.; Friedrich, A.; Kondratenko, E.; Polte, J.; Werwatz, A.; Kraehnert, R. A meta-analysis of catalytic literature data reveals property-performance correlations for the OCM reaction. *Nat. Commun* 2019, 10, 441.
- 24 Mine, S.; Takao, M.; Yamaguchi, T.; Toyao, T.; Maeno, Z.; Hakim Siddiki, S. M. A.; Takakusagi, S.; Shimizu, K.-i.; Takigawa, I. Analysis of Updated Literature Data up to 2019 on the Oxidative Coupling of Methane Using an Extrapolative Machine-Learning Method to Identify Novel Catalysts. *Chem-CatChem* 2021, 13, 3636–3655.
- 25 Takahashi, K.; Miyazato, I.; Nishimura, S.; Ohyama, J. Unveiling Hidden Catalysts for the Oxidative Coupling of Methane based on Combining Machine Learning with Literature Data. ChemCatChem 2018, 10, 3223–3228.
- 26 Takahashi, K.; Takahashi, L.; Le, S. D.; Kinoshita, T.; Nishimura, S.; Ohyama, J. Synthesis of Heterogeneous Catalysts in Catalyst Informatics to Bridge Experiment and High-Throughput Calculation. *JACS* 2022, 144, 15735–15744.
- 27 Ugwu, L.; Morgan, Y.; Ibrahim, H. Enhancing Ethene Pro-

- duction through Low-Temperature Oxidative Coupling of Methane: Leveraging DFT and Data Analysis for Crafting Innovative and Efficient Catalyst Compositions. *Ind. Eng. Chem. Res.* **2023**, *62*, 19658–19673.
- 28 Ohyama, J.; Nishimura, S.; Takahashi, K. Data Driven Determination of Reaction Conditions in Oxidative Coupling of Methane via Machine Learning. *ChemCatChem* **2019**, *11*, 4307–4313.
- 29 Chen, K.; Tian, H.; Li, B.; Rangarajan, S. A chemistry-inspired neural network kinetic model for oxidative coupling of methane from high-throughput data. *AIChE Journal* **2022**, 68, e17584.
- 30 Nguyen, T. N.; Nakanowatari, S.; Nhat Tran, T. P.; Thakur, A.; Takahashi, L.; Takahashi, K.; Taniike, T. Learning Catalyst Design Based on Bias-Free Data Set for Oxidative Coupling of Methane. *ACS Catal.* **2021**, *11*, 1797–1809.
- 31 Ohyama, J.; Kinoshita, T.; Funada, E.; Yoshida, H.; Machida, M.; Nishimura, S.; Uno, T.; Fujima, J.; Miyazato, I.; Takahashi, L.; Takahashi, K. Direct design of active catalysts for low temperature oxidative coupling of methane via machine learning and data mining. *Catal. Sci. Technol.* **2021**, *11*, 524–530.
- 32 Nishimura, S.; Le, S. D.; Miyazato, I.; Fujima, J.; Taniike, T.; Ohyama, J.; Takahashi, K. High-throughput screening and literature data-driven machine learning-assisted investigation of multi-component La2O3-based catalysts for the oxidative coupling of methane. *Catal. Sci. Technol.* **2022**, *12*, 2766–2774.
- 33 Alturkistani, S.; Wang, H.; Gautam, R.; Sarathy, S. M. Importance of Process Variables and Their Optimization for Oxidative Coupling of Methane (OCM). *ACS Omega* **2023**, *8*, 21223–21236.
- 34 von Meyenn, C. L. M.; Palkovits, S. Prediction of suitable catalysts for the OCM reaction by combining an evolutionary approach and machine learning. *Energy Adv.* **2023**, *2*, 691–700.
- 35 Thien, C. Y.; Mohamed, A. R.; Bhatia, S. Process optimization of oxidative coupling of methane for ethylene production using response surface methodology. *JCTB* **2007**, *82*, 81–91.
- 36 Wang, H.; Shao, C.; Gascon, J.; Takanabe, K.; Sarathy, S. M. Noncatalytic Oxidative Coupling of Methane (OCM): Gas-Phase Reactions in a Jet Stirred Reactor (JSR). *ACS Omega* **2021**, *6*, 33757–33768.
- 37 Zohour, B.; Noon, D.; Senkan, S. New Insights into the Oxidative Coupling of Methane from Spatially Resolved Concentration and Temperature Profiles. *ChemCatChem* 2013, 5, 2809–2812.
- 38 Kuś, S.; Otremba, M.; Taniewski, M. The catalytic performance in oxidative coupling of methane and the surface basicity of La2O3, Nd2O3, ZrO2 and Nb2O5. *Fuel* **2003**, *82*, 1331–1338.
- 39 Choudhary, V. R.; Rane, V. H. Oxidative coupling of methane over La2O3. Influence of catalyst preparation on surface properties and steady and oscillating reaction behaviour. *J. Chem. Soc., Faraday Trans.* **1994**, *90*, 3357–3365.
- 40 Pedregosa, F. et al. Scikit-learn: Machine Learning in Python. *JMLR* **2011**, *12*, 2825–2830.

- 41 Nishimura, S.; Li, X.; Ohyama, J.; Takahashi, K. Leveraging machine learning engineering to uncover insights into heterogeneous catalyst design for oxidative coupling of methane. *Catal. Sci. Technol.* **2023**, *13*, 4646–4655.
- 42 XenonPy. https://xenonpy.readthedocs.io/en/latest/, Accessed: September 17, 2023.
- 43 Garcia-Escobar, F.; Taniike, T.; Takahashi, K. MonteCat: A Basin-Hopping-Inspired Catalyst Descriptor Search Algorithm for Machine Learning Models. *JCIM* **2024**, *64*, 1512–1521.
- 44 Onsager, O.; Lødeng, R.; Søraker, P.; Anundskaas, A.; Helleborg, B. The homogeneous gas phase oxidation of methane and the retarding effect of basic/inert surfaces. *Catal. Today* **1989**, *4*, 355–363.
- 45 Qiu, X.-q.; Zhu, Q.-m.; Wong, N.-b.; Tin, K.-c. Catalytic contribution of reactor wall materials on oxidative coupling of methane. *JCTB* **1996**, *65*, 380–384.
- 46 Wang, S.; Li, S.; Dixon, D. A. Mechanism of selective and complete oxidation in La2O3-catalyzed oxidative coupling of methane. *Catal. Sci. Technol.* **2020**, *10*, 2602–2614.

Data Availability

All data used in this work is provided in the supporting information.